Title: Remarkable Thermal Conductivity Enhancement in Carbon-Based Ionanofluids: Effect of Nanoparticle Morphology

Author: Bertrand Jóźwiak, Grzegorz Dzido, Edward Zorębski, Anna Kolanowska, Rafał Jędrysiak, Justyna Dziadosz, Marcin Libera, Sławomir Boncel, Marzena Dzida

Citation style: Jóźwiak Bertrand, Dzido Grzegorz, Zorębski Edward, Kolanowska Anna, Jędrysiak Rafał, Dziadosz Justyna, Libera Marcin, Boncel Sławomir, Dzida Marzena. (2020). Remarkable Thermal Conductivity Enhancement in Carbon-Based Ionanofluids: Effect of Nanoparticle Morphology. “ACS Applied Materials and Interfaces” (Vol. 12 (2020), Iss. 34, s. 38113–38123), doi 10.1021/acsami.0c09752

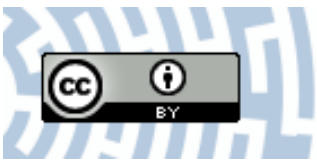

ACS APPLIED MATERIALS & INTERFACES

www.acsami.org

Research Article

Remarkable Thermal Conductivity Enhancement in Carbon-Based Ionanofluids: Effect of Nanoparticle Morphology

Bertrand Jóźwiak, Grzegorz Dzido, Edward Zorębski, Anna Kolanowska, Rafał Jędrysiak, Justyna Dziadosz, Marcin Libera, Sławomir Boncel,* and Marzena Dzida*

Cite This: *ACS Appl. Mater. Interfaces* 2020, 12, 38113–38123

Read Online

ACCESS | Metrics & More | Article Recommendations | Supporting Information

ABSTRACT: Transfer of the excellent intrinsic properties of individual carbon nanoparticles into real-life applications of the corresponding heat transfer fluids remains challenging. This process requires identification and quantification of the nanoparticle–liquid interface. Here, for the first time, we have determined geometry and properties of this interface by applying transmission electron cryomicroscopy (cryo-TEM). We have systematically investigated how the particle morphology of carbon-based nanomaterials affected the thermal conductivity, specific isobaric heat capacity, thermal diffusivity, density, and viscosity of ionanofluids and/or bucky gels, using a wide range of fillers, especially single-walled carbon nanotubes (SWCNTs) and multiwalled carbon nanotubes (MWCNTs), both with extreme values of aspect ratio (length to diameter ratio) from 150 to 11 000. Accordingly, hybrid systems composed of various carbon nanomaterials and ionic liquid, namely 1-ethyl-3-methylimidazolium thiocyanate [EMIM][SCN], were prepared and characterized. Most of the analyzed nanodispersions exhibited long-term stability even without any surfactant. Our study revealed that the thermal conductivity could be remarkably improved to the maximum values of 43.9% and 67.8% for ionanofluid and bucky gel (at 1 wt % loadings of MWCNTs and SWCNTs), respectively, compared to the pristine ionic liquid. As a result, the model proposed by Murshed and co-workers has been improved for realistic description of the concentration-dependent thermal conductivity of such hybrid systems. The obtained results undoubtedly indicate the potential of ionanofluids and bucky gels for energy management.

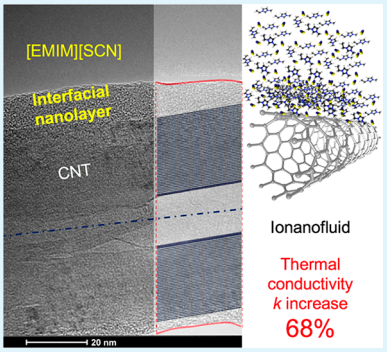

KEYWORDS: *ionanofluids, thermal conductivity, heat transfer fluids, interfacial nanolayer, cryo-TEM*

INTRODUCTION

Increasing industrialization, as well as a better standard of living, has contributed to the increase in energy demand and miniaturization of heat transfer systems. This trend stimulates the quest for innovative heat transfer fluids with improved thermophysical properties. The application of such functional materials is beneficial for enhanced conservation, transportation, or conversion of energy. These energy processing areas remain one of the most important technical challenges in power generation, solar thermal systems, automobiles, precision manufacturing, microelectronics, and high-power laser optics.[1] One of the strategies to enhance the thermal conductivity of liquids is the addition of solid, thermally conductive nanoparticles. This solution was introduced by Maxwell more than a century ago.[2] In turn, the concept of ionanofluids (INFs) as dispersions of nanometer-sized solid materials (spheres, fibers, wires, tubes, sheets, etc.) in ionic liquids (ILs) was proposed in 2009 by Nieto de Castro et al.[3] INFs have rapidly gained importance in multiple fields, such as nanotechnology, chemical, and mechanical engineering. Inter alia, INFs proved to be efficient heat transfer fluids with thermal conductivity and diffusivity significantly higher than that of base fluids.[4] ILs that form the continuous phase of INFs have several advantages: wide liquid range, high chemical and thermal stabilities, and very low vapor pressure. Especially important is that ILs have optimal thermophysical properties as a base fluid for heat transfer systems, studied in detail by França et al.,[5] Tenney et al.,[6] Chernikova et al.,[7] and our group.[8,9] Moreover, a great diversity of results from a number of possible anion–cation combinations for ILs[10] makes it possible to design a structure with optimal properties, allowing many functionalities for very specific purposes.[11] Thus, the use of ILs as a continuous phase of nanodispersions means that the INFs can be designed to meet any specific application or task requirement.[12] Cyano alkylimidazolium ILs such as [EMIM][SCN] seem to be particularly useful because of their low viscosity and acceptable ecotoxicity.[13] Moreover, [EMIM][SCN] was denoted as an effective electrolyte for solar cells applications.[14]

Received: May 28, 2020
Accepted: July 10, 2020
Published: July 10, 2020

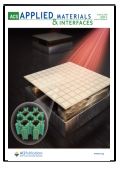

Table 1. Characteristics of Carbon-Based Nanomaterials Used in This Study

name	dimensionality	average length (μm)	average diameter (nm)	aspect ratio (−)	specific surface area ($m^2 \cdot g^{-1}$)	density ($g \cdot cm^{-3}$)	carbon purity (%)
fullerene soot, Sigma-Aldrich	0D	N/A	N/A	N/A	N/A	1.7	7[a]
Tuball SWCNTs, OCSiAl	1D	5.0	2.0	2500	750	1.8	85
in-house 7 h MWCNTs	1D	440	60−80	6300	35	2.1	98
in-house 16 h MWCNTs	1D	770	60−80	11000	22	2.1	98
NC7000 MWCNTs, Nanocyl[b]	1D	1.5	9.5	150	300	1.75	90
CheapTubes MWCNTs, Cheap Tubes Inc.	1D	10−30	20−40	700	60	2.1	95
graphene CamGraph G1, Cambridge Nanosystems	2D	475[c]	1.0[d]	475	320	2.1	98
activated carbon, POCH	3D	N/A	N/A	N/A	N/A	2.0	98
graphite flakes, Sigma-Aldrich	3D	N/A	N/A	N/A	N/A	1.9	99

[a]Including 76% of C_{60} and 22% of C_{70}. [b]Purified by concentrated NaOH and HCl. [c]Lateral size. [d]Thickness.

The dispersed (solid) phase of INFs is usually composed of polymeric, metallic, organic, and inorganic nanomaterials.[15] The advanced synthesis of nanomaterials makes it possible to obtain their desired size, shape, composition, and surface chemistry, as well as to control their dispersion properties.[1] Thermophysical and rheological properties of INFs strongly depend on the above-mentioned parameters of fillers. Carbon-based sp^2-nanomaterials, such as zero-dimensional (0D) fullerenes, 1D nanotubes, 2D graphene, and 3D graphite, are probably the most promising materials for this purpose because of their excellent properties, e.g., high thermal conductivity coupled with high aspect ratio and low density.[16]

The systems of ILs with carbon nanomaterials have been intensively studied, starting with "bucky gels" discovered in 2003 by Fukushima et al.[17] and described as soft functional materials.[18] It is now clear that INFs possess great potential in many innovative applications related to thermal management and energy harvesting.[19] The most-studied property of INFs is their thermal conductivity because it is the key parameter to evaluate thermal performance. In most cases, the thermal conductivity of INFs was improved by increasing the concentration of solid nanoparticles.[13,19−22] The highest thermal conductivity enhancement of 43.2% was found for an INF composed of 1-ethyl-3-methylimidazolium acetate [EMIM][OAc] + 5 wt % graphene nanoplatelets.[23] High enhancements of 35% and 32.3% were also reported for INFs composed of 1-butyl-3-methylimidazolium bis-(trifluoromethylsulfonyl)imide [BMIM][NTf_2] + 1 wt % MWCNTs in the temperature range from 20 to 80 °C,[24] and [EMIM][SCN] + 1 wt % MWCNTs at 70.5 °C,[13] respectively. Baytubes MWCNTs with an outer mean diameter of 13−16 nm and length of 1−10 μm were used in both cases.[13,24] Moreover, the literature research shows no effect or even a decrease in thermal conductivity with a temperature increase.[13,19−22]

To predict the thermal conductivity of INFs, several mathematical models were used. Conventional models (Maxwell, Hamilton−Crosser, etc.) significantly underestimated the thermal conductivity, as they were developed for milli- or microsized particles.[22] In the literature, there is only one model dedicated strictly to INFs, but it is a simple modification of the Maxwell model.[25] The more complex approach was proposed by Murshed et al.[26] Their model proved to be very useful for conventional nanofluids by considering nanoparticle size (shape) and interfacial nanolayer at the solid−liquid interface. The interfacial nanolayer is a cluster of ordered atoms of base fluid near the boundary of solid nanoparticle, formed due to strong interatomic/intermolecular attractions.[27] This nanolayer exhibits characteristics of an organized solid-like structure.[13] Thus, it can be considered as a thermal bridge between base liquid and solid nanoparticle, increasing the thermal conductivity of nanofluids/ionanofluids.[28,29] The molecular dynamics studies showed that several solvation layers are near the nanocarbon−IL interface, and both cations and anions were found in the first interfacial layer interacting with the carbon nanomaterials.[14,30] Moreover, molecular dynamics studies showed that IL forms different structures inside of CNTs depending on nanotubes diameter.[14,30] Until now, virtually all mathematical models used to determine the thermal conductivity of nanofluids/ionanofluids assumed that the thickness of interfacial nanolayer is between 0.5 and 2 nm.[26,31,32] Some molecular dynamics studies showed that the thickness of the interfacial nanolayer is around 0.9 nm for cyano-based INFs[30] and 1 nm for Au-liquid Ar system.[33] The interfacial nanolayer characterizes enhanced thermal conductivity with respect to the bulk liquid. For instance, França et al.[30] reported that the thermal conductivity of the interfacial nanolayer was 1.1−1.4 times higher than the thermal conductivity of the ionic liquid in the case of various graphene-based INFs. Liang and Tsai[33] claimed that the thermal conductivity of the interfacial nanolayer was 1.6−2.5 times higher than thermal conductivity of the base fluid for Au nanodispersions in liquid argon. Similarly, Pal[34] stated that the thermal conductivity of the interfacial nanolayer was 2.1 and 2.6 times higher than the thermal conductivity of ethylene glycol for Cu−ethylene glycol and TiO_2−ethylene glycol nanofluids, respectively. Ribeiro et al.[24] characterized an ionanofluid composed of 1-butyl-3-methylimidazolium tetrafluoroborate [BMIM][BF_4] + 1 wt % MWCNTs by TEM for the first time. They showed that [BMIM][BF_4] + 1 wt % MWCNTs has a structure with nanotube random coils, surrounded by an interfacial layer of the IL, generating aggregates that possibly justify the enhanced heat transfer. They pointed out that theoretical predictions are extremely sensitive to the thickness of the interfacial layer. Thus, extreme care should be justified in determining the proper structure of the ionanofluid.[24]

In contrast to changes observed in thermal conductivity, the influence of carbon nanoparticles on the isobaric heat capacity of INFs is not clear. For example, the aforementioned INF composed of [EMIM][OAc] + 5 wt % GNPs showed the highest thermal conductivity increase with a simultaneous isobaric heat capacity decrease.[23] Generally, the literature

https://dx.doi.org/10.1021/acsami.0c09752
ACS Appl. Mater. Interfaces 2020, 12, 38113−38123

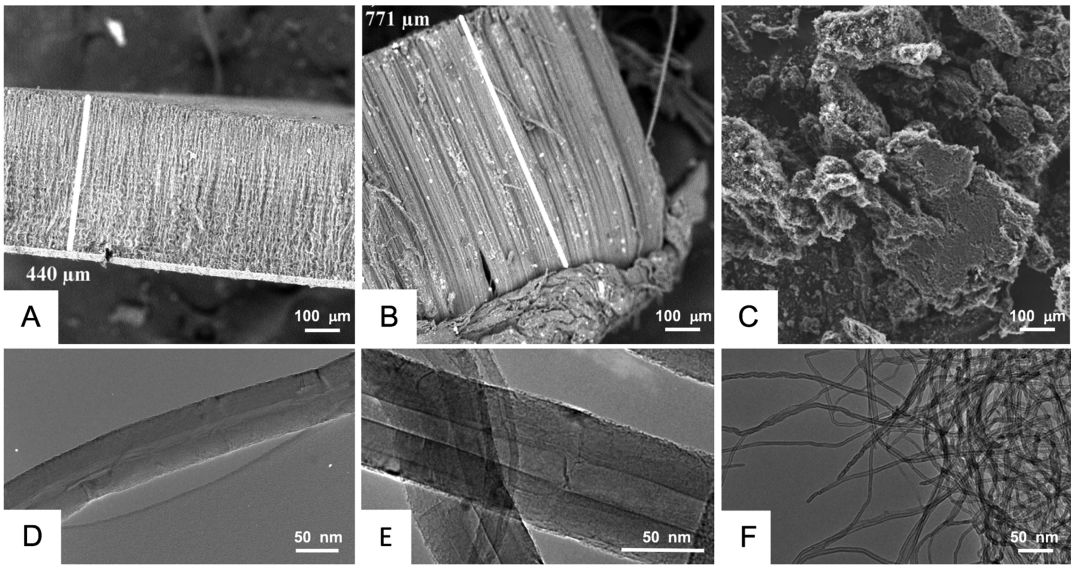

Figure 1. SEM images of MWCNTs: (A) in-house 7 h, (B) in-house 16 h, and (C) purified Nanocyl NC7000; the insets in panels A and B show highly aligned MWCNT arrays where height corresponds to the length of the individual nanotube. TEM images of MWCNTs: (D) in-house 7 h, (E) in-house 16 h, and (F) purified Nanocyl NC7000; the dark areas in panels D and E correspond to iron phases (α-Fe, γ-Fe, and Fe_3C) residues, nonremovable via wet-chemistry techniques.

reports are not consistent, often contradictory, and indicate that the addition of nanoparticles to the base IL caused both an increase[4,35−38] and a decrease[39,40] or no influence on the isobaric heat capacity of INFs.[41]

The aim of this work was to cross-investigate the influence of various carbon nanomaterials on the thermal conductivity of low-viscosity cyano alkylimidazolium-based INFs and to determine thermal features of the interfacial nanolayer for the most promising INFs using the model developed by Murshed et al.[26] Here, for the first time, we have experimentally determined the actual thickness of the interfacial nanolayer by applying unique transmission electron cryomicroscopy (cryo-TEM). The other objective was to determine the thermophysical and rheological properties of selected INFs, namely specific isobaric heat capacity, thermal diffusivity, density, and viscosity, as their figure-of-merit toward real-life application.

EXPERIMENTAL SECTION

Materials. Nine carbon-based nanomaterials of various "dimensionality" and morphological features (Table 1) were used to prepare INFs. Most of them were purchased from international manufacturers (Sigma-Aldrich, St. Louis, MO; OCSiAl, Luxembourg; Nanocyl, Belgium; Cheap Tubes Inc., Grafton, VT; Cambridge Nanosystems, UK; and POCH, Poland). Due to the high aspect ratio, over half of the studied nanomaterials were 1D carbon nanotubes (CNTs), both single-walled (SWCNTs) and multiwalled (MWCNTs). Apart from commercial CNTs, two types of in-house MWCNTs, i.e., synthesized in our laboratory via catalytic chemical vapor deposition (c-CVD), were also applied. In-house MWCNTs ("7 h" and "16 h") were prepared using a procedure presented in our previous paper.[42] Symbols "7 h" and "16 h" refer to the duration of the c-CVD process. As other nanocarbon representatives, fullerene (0D), graphene (2D), activated carbon, and graphite (both 3D) were studied.

SEM images obtained by JSM-634OF FEG (JEOL, Japan) at 5 kV and TEM micrographs acquired using 200 CX (JEOL, Japan) at 200 kV of in-house and commercial (purified via our protocol) nanomaterials used in this study are presented in Figure 1. Importantly, in-house MWCNTs 7 h and 16 h did not differ in single nanotube morphology but only in the nanotube length. Hence, their further behavior could be easily compared. Moreover, both in-house MWCNTs contained encapsulated iron-based phases as residues from the c-CVD synthesis[43] which were nonremovable by wet chemistry without destruction of nanotube morphology but required high-temperature evaporation at 1900 °C in argon.[44]

The base fluid in INFs was 1-ethyl-3-methylimidazolium thiocyanate, [EMIM][SCN]. The rationale behind its selection was the lowest viscosity among all known ILs,[45] as well as relatively low ecotoxicity.[13] [EMIM][SCN] was purchased from Sigma-Aldrich and used without purification. A brief specification of the studied IL is contained in Table S1 in Supporting Information. The quality of [EMIM][SCN] was confirmed by comparing the density, as well as the refractive index measured by means of an Abbe refractometer RL3 (PZO, Poland), with values reported in the literature. The refractive index at 25 °C was equal to 1.5496 ± 0.0004. The consistency between experimental values and data available in the literature was fully acceptable; the relative deviations were −0.067% and −0.12% (Table S2 in Supporting Information). Similarly, the agreement between the density value obtained in this work (Table S2) and data available in the literature was also satisfactory; the relative deviations were in the range from −0.027% to −0.16%. However, for another rank of [EMIM][SCN], the relative deviations were higher and on the order of −0.63% (see Table S2).

Sample Preparation. INFs were prepared via the two step-procedure, i.e., by dispersing different weight concentrations (0.01%, 0.1%, 0.25%, 0.5%, 0.75%, and 1%) of carbon nanomaterials in IL. The samples (20 mL) were prepared using analytical balance XA 60/220 (Radwag, Poland) with an accuracy of $\pm 1 \times 10^{-4}$ g. All samples were sonicated for 10 min using a UP200 St sonicator (Hielscher Ultrasonics GmbH, Germany) in order to apply the same protocol of preparation. The 200 W ultrasound power generator was operated at 26 kHz frequency with a 100% amplitude (nominal values). An increase in temperature of the samples was slowed by the use of a cooling bath with ethylene glycol.

Cryogenic Transmission Electron Microscopy (Cryo-TEM). Cryo-TEM micrographs were obtained using a Tecnai F20 TWIN microscope (FEI Company, Hillsboro, OR) equipped with a field emission gun operating at an acceleration voltage of 200 kV. Images were recorded on the Eagle 4k HS camera (FEI Company) and processed with TIA software. Specimens for investigation were prepared through vitrification by plunge freezing of the aqueous (HPLC-grade water) suspensions on copper grids (300 mesh) with

https://dx.doi.org/10.1021/acsami.0c09752
ACS Appl. Mater. Interfaces 2020, 12, 38113−38123

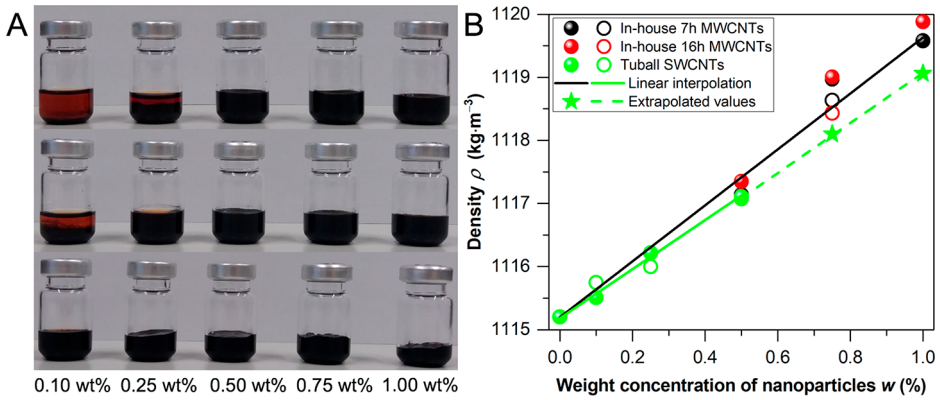

Figure 2. (A) The pictures of INFs composed of (top) [EMIM][SCN] + in-house 7 h MWCNTs, (middle) [EMIM][SCN] + in-house 16 h MWCNTs, and (bottom) [EMIM][SCN] + Tuball SWCNTs, taken thirteen months after preparation (date of preparation was April 15, 2019). (B) Density of selected, stable ionanofluids composed of [EMIM][SCN] + in-house 7 h MWCNTs, [EMIM][SCN] + in-house 16 h MWCNTs, and [EMIM][SCN] + Tuball SWCNTs. Filled symbols: measurements immediately after sonication; empty symbols: measurements nine months after sample preparation; solid lines: linear interpolation; dashed line: extrapolated values.

holey carbon film Quantifoil R 2/2 (Quantifoil Micro Tools GmbH, Germany). Prior to use, the grids were activated for 30 s in oxygen plasma using a Femto plasma cleaner (Diener Electronic, Germany). Suspensions of the samples (2.1 μL) were put onto the grid, blotted using dedicated filter paper, and immediately frozen by plunging in liquid ethane utilizing a fully automated and environmental controlling blotting device, Vitrobot Mark IV (FEI Company). Specimens after vitrification were kept under liquid nitrogen until they were inserted into a cryo-TEM-holder Gatan 626 (Gatan Inc., Pleasanton, CA) and analyzed in the TEM at −178 °C.

Thermal Conductivity Measurements. The thermal conductivity of INFs was measured using a KD2 Pro Thermal Properties Analyzer (Decagon Devices Inc., Pullman, WA) with a single needle KS-1 sensor of 1.3 mm diameter and 60 mm length. KD2 Pro works based on the hot-wire technique in which a thin (electrically insulated) conducting wire immersed in the test medium is used as the line heat source and temperature sensor.[46] The KS-1 needle generates a very small amount of heat to the sample during measurement, minimizing problems with free convection. The instrument has a specified uncertainty of ±5%. More details about the KD2 Pro analyzer can be found in its user manual. The instrument was calibrated using a verification standard of glycerin supplied by the producer (Decagon Devices Inc.) with a known thermal conductivity of 0.285 $W \cdot m^{-1} \cdot K^{-1}$ ± 5% at 20 °C. Open Bath Circulator ED-5 (Julabo GmbH, Germany) with ethylene glycol as the working liquid was used for maintaining a constant temperature of samples (25 °C). A short read time of 60 s for the KS-1 sensor (covering the period of temperature equilibration, heating, cooling, and recalculation of the obtained results), low temperature (<50 °C), and high viscosity of INFs (>20 mPa·s) effectively prevented free convection. Three readings with a correlation value of $R^2 \geq 0.9999$ were recorded at the 15 min interval and then averaged to get the thermal conductivity of each sample.

Heat Capacity Measurements. Specific isobaric heat capacity was measured using a differential temperature-scanning microcalorimeter (DSC) from Calpresdat (Poland). The main part of the DSC was a semiconductor differential heat flux detector of the Tian-Calvet type. The time constant of the device was equal to 9.2 s. A full metal cylinder with a wall thickness of 0.2 mm was used as the reference vessel. The samples were weighted with the accuracy of ±6 × 10^{-4} g using a DV215CD analytical balance (Ohaus, Parsippany, NJ). The same three-step temperature program, including (i) isothermal phase (5 × 10^3 s) at starting temperature, (ii) temperature scanning at a rate of 1 $mK \cdot s^{-1}$ in the heating direction, and (iii) isothermal phase (5 × 10^3 s) at the final temperature, was always applied for the empty measuring vessel, the measuring vessel with the reference sample, and the measuring vessel with the sample under study. The reference standard was pure (99.5%) anhydrous 1-butanol (Sigma-Aldrich, SureSeal). Isobaric heat capacity data of 1-butanol reported by Zorębski and Góralski[47] were used as reference values. The apparatus was tested using *n*-hexane and benzene as described in ref 48. Based on the calibration procedure, test runs, measurement procedure, sample property, temperature measurement uncertainty, and neglecting vapor correction, the expanded uncertainty (coverage factor 2.0, confidence level 0.95) of the isobaric heat capacity obtained in this work was estimated to be of ±2%. More details concerning DSC and procedures used can be found in the literature.[48,49]

Density Measurements. The density of IL was measured by means of vibrating-tube densimeter DMA 5000M, while the density of INFs was determined using a DMA 5000 densimeter (both from Anton Paar, Austria). The devices were calibrated with dry air and redistilled water (its electrolytic conductivity was equal to 1 × 10^{-4} $S \cdot m^{-1}$ at 25 °C) via extended calibration. The viscosity corrections were automatically made. Expanded density uncertainties were equal to ±0.1 $kg \cdot m^{-3}$ and ±0.3 $kg \cdot m^{-3}$ for measurements of pristine IL and INFs, respectively. The temperature was measured with an expanded uncertainty of ±0.02 °C.

Viscosity Measurements. Rheological properties of base IL and INFs were investigated using a rotary viscometer LV DV-II+Pro (Brookfield Engineering, Middleboro, MA) with a DIN-86 or DIN-87 spindle immersed in a sample. The device was equipped with a ED-5 temperature-controlled open bath circulator (Julabo GmbH, Germany) containing ethylene glycol. The main part of the measurements was conducted at a constant temperature of 25 °C with fluctuations that did not exceed ±0.1 °C. Each sample was stabilized at the given temperature for a minimum of 30 min until thermal equilibrium was reached. The temperature was measured using a resistance sensor (RTD) with an expanded uncertainty of ±1 °C and a resolution of 0.1 °C. The uncertainty of viscosity measurements was equal to ±3.9% and ±5.4% for spindles DIN-86 and DIN-87, respectively.

RESULTS AND DISCUSSION

The INF is a thermodynamically stable dispersion of nanoparticles in the IL. We have noticed that nanodispersions composed of [EMIM][SCN] + Tuball SWCNTs at a weight percentage above 0.25 wt % formed bucky gels. Importantly, the INFs were found to be stable, so no surfactant was added. The long-term stability at 22 °C was examined by visual observation of sedimentation for nanodispersions composed of [EMIM][SCN] and in-house 7 h MWCNTs, in-house 16 h MWCNTs, or Tuball SWCNTs, as they were characterized by the highest thermal conductivity enhancement. The photo-

https://dx.doi.org/10.1021/acsami.0c09752
ACS Appl. Mater. Interfaces 2020, 12, 38113−38123

graphs of the above-mentioned hybrid nanosystems, taken thirteen months after preparation, are presented in Figure 2A. Generally, no sedimentation was observed for almost all samples except for INFs composed of [EMIM][SCN] + 0.1 or 0.25 wt % in-house MWCNTs 7 h and 16 h (Figure 2A, top and middle panels). In the case of INF containing [EMIM]-[SCN] + 0.1 wt % Tuball SWCNTs, a thin orange ring of IL could be seen on the surface of the sample (Figure 2A, bottom panel). The density of INFs composed of [EMIM][SCN] + in-house 7 h MWCNTs, as well as [EMIM][SCN] + in-house 16 h MWCNTs, was almost the same (Figure 2B). The length of studied in-house MWCNTs did not affect the density and stability of the samples. The differences between density measured immediately after sonication and nine months after sample preparation did not exceed 0.6 kg·m^{-3}. Additionally, for stable INFs, we determined the dependence of density as a function of the weight concentration of nanoparticles (Figure 2B) and found an excellent linear correlation. The maximum deviation did not exceed 0.15 kg·m^{-3}. The calculated coefficient of determination R^2 was close to unity and took values between 0.975 and 0.996, for in-house and Tuball-based INFs, respectively.

The thermal conductivity of pristine [EMIM][SCN] obtained in this work at 25 °C was in excellent agreement with the experimental data reported by França et al.,[13] i.e., the relative deviation was lower than the declared measurement uncertainty and equal to 4%. Details are presented in Table S3 in Supporting Information. Our studies have shown that thermal conductivity was strongly dependent on the type of nanostructures dispersed in the IL (see Figure 3 and Table S4 in Supporting Information). Zero-dimensional (0D) fullerene soot, 3D graphite flakes, and 3D activated carbon practically did not improve the thermal conductivity of the INFs, regardless of their concentration. The influence of 2D graphene on the thermal properties of the INFs was slightly higher. In this case, the increase in thermal conductivity was linear and reached a maximum of 7.9% for 1 wt % loading of nanoparticles. Nonetheless, the INFs with 0D, 2D, and 3D carbon-based nanomaterials were not found to be very promising heat transfer media, probably due to the geometry of the dispersed phase preventing the formation of conducting pathways. The thermal conductivity enhancement obtained by the addition of 1D carbon nanoallotropes into [EMIM][SCN] was much more significant. With such an ultrahigh thermal conductivity of CNTs, the corresponding INFs exhibited much higher thermal features as compared to base ILs or INFs containing other carbon nanomaterials.

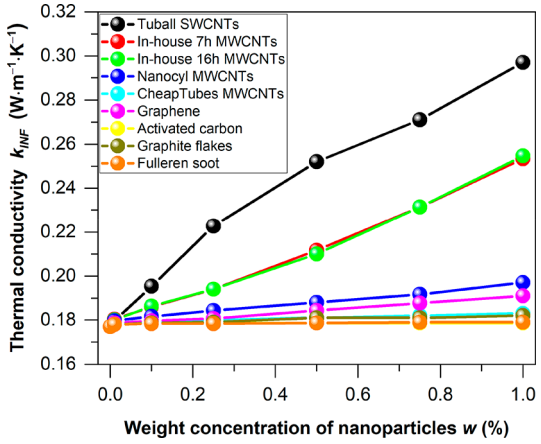

Figure 3. Thermal conductivity of INFs at 25 °C as a function of weight concentration of carbon-based nanomaterials.

The thermal conductivity of INFs composed of [EMIM]-[SCN] + 0.5 or 1 wt % Nanocyl NC7000 obtained in this work was very close to the thermal conductivity of INFs composed of [EMIM][SCN] + 0.5 or 1 wt % Baytubes C150 HP MWCNTs reported by França et al.[13] (see Table S4), i.e., they differed by no more than 1.5%. Indeed, Nanocyl NC7000 and Baytubes C150 HP MWCNTs are of comparable morphology because Baytubes C150 HP MWCNTs are characterized by only a slightly larger outer mean diameter (13−16 nm) and length (1−10 μm). In general, there was observed a remarkable, almost linear increase in the thermal conductivity of INFs with increasing weight concentration of CNTs. The highest (67.8%) enhancement of the thermal conductivity of the INFs was observed at 1 wt % loading of commercial Tuball SWCNTs. Among all the examined MWCNTs, those produced in our laboratory were found to be the most effective in the enhancement of thermal conductivity. The maximum enhancement for INFs with 1 wt % loading of in-house MWCNTs 7 h and 16 h was equal to 43.1% and 43.9%, respectively, which are remarkably higher values in comparison with the literature data.[13,23,24] The commonly quoted values for thermal conductivity of individual CNTs at room temperature are 3000 W·m^{-1}·K^{-1} and 3500 W·m^{-1}·K^{-1} for MWCNTs and SWCNTs,[50] respectively; hence, we have obtained synergetic and so far unrivaled enhancement in thermal conductivity of INFs in comparison with literature data.

Furthermore, it was noted that the thermal conductivity of INFs increased with an increasing product of aspect ratio and specific surface area ($A \times S$) of CNTs. The latter parameter can serve indeed as a general indicator of the effectivity potential. Hence, it can be approximately treated as a figure-of-merit for CNT fillers of INFs (see Table 2). The enhancement of thermal features of INFs in the case of SWCNTs and MWCNTs can be associated with CNTs acting as "thermal bridges" in ILs, generating preferential paths for the heat transfer. The interactions between ILs and CNTs could also modify the structure of liquid phase which led to the increase in thermal conductivity of INFs including a different structure in the interfacial nanolayer.[20,24]

Apart from thermal conductivity, the energy storage density (also known as volumetric heat capacity) is another important parameter for heat transfer systems. It is a product of specific isobaric heat capacity and density ($C_p\rho$). The higher $C_p\rho$ values result in a lower required volume of thermal fluids. Typically, the energy storage density of ILs is high and lies in the range of 1.5−2.3 MJ·m^{-3}·K^{-1}.[51,52] Importantly, no effect of carbon nanomaterial additives on $C_p\rho$ was founded in this work because the specific isobaric heat capacity and the density of INFs changed in opposite directions, e.g., the INFs exhibited lower C_p (−0.36%) and higher ρ (+0.39%) compared to pristine IL, or a negligible enhancement of C_p (+1.4%) and ρ (+0.34%) (Tables S5 and S6 in Supporting Information) was observed. Thus, the energy storage density $C_p\rho$ was equal to 1.9 MJ·m^{-3}·K^{-1} for both the IL and the INFs. The ratio of thermal conductivity and energy storage density (volumetric heat capacity) yields thermal diffusivity $\alpha = k(C_p\rho)^{-1}$. For the investigated samples, the change in thermal diffusivity was determined by the change in thermal

https://dx.doi.org/10.1021/acsami.0c09752
ACS Appl. Mater. Interfaces 2020, 12, 38113−38123

Table 2. Main Morphological Parameters of CNTs Affecting the Thermal Conductivity of INFs

Type of CNTs	Aspect ratio (A) (−)	Specific surface area (S) ($m^2 \cdot g^{-1}$)	$A \cdot S$ ($m^2 \cdot g^{-1}$)
Tuball SWCNTs, OCSiAl	2500	750	$1.88 \cdot 10^6$
In-house 16h MWCNTs	11000	22	$2.42 \cdot 10^5$
In-house 7h MWCNTs	6300	35	$2.21 \cdot 10^5$
NC7000 MWCNTs, Nanocyl	150	300	$4.50 \cdot 10^4$
CheapTubes MWCNTs, Cheap Tubes Inc.	700	60	$4.20 \cdot 10^4$

Enhancement in thermal conductivity of INFs

conductivity (compare Table S4 and Table S5). Thus, the thermal diffusivity of the studied IL and INFs was higher as compared to other ILs and INFs in the literature, as in the case of thermal conductivity. The details of the density and isobaric heat capacity results are presented in section S2 in Supporting Information.

We considered that the interfacial nanolayer had a fundamental contribution to the thermal conductivity of INFs. Thus, the knowledge of nanolayer thickness (h_{IN}) is critical for the understanding of the physicochemical properties of INFs, including the implementation of the most complex theoretical models in the prediction of those properties for a variety of INFs. The influence of this factor was explored by a comprehensive modeling procedure. The experimental data of INFs with the highest thermal conductivity k_{INF}, i.e., nanodispersions containing cylindrically shaped CNTs, were described using the model developed by Murshed et al.,[26] which is expressed by

$$k_{INF} = k_{IL} \times \frac{\phi\omega(k_{CNT} - \omega k_{IL})(\gamma_1^2 - \gamma^2 + 1) + (k_{CNT} + \omega k_{IL})\gamma_1^2[\phi\gamma^2(\omega - 1) + 1]}{\gamma_1^2(k_{CNT} + \omega k_{IL}) - (k_{CNT} - \omega k_{IL})\phi(\gamma_1^2 + \gamma^2 - 1)}$$

with

$$\omega = \frac{k_{IN}}{k_{IL}}, \quad \gamma = 1 + \frac{h_{IN}}{r_{CNT}}, \quad \gamma_1 = 1 + \frac{h_{IN}}{2r_{CNT}}$$

where ϕ is the dimensionless volume fraction of CNTs, k_{IL} is the thermal conductivity of IL (Table S4), k_{IN} is the thermal conductivity of the interfacial nanolayer, k_{CNT} is the thermal conductivity of an individual solid nanoparticle (3000 $W \cdot m^{-1} \cdot K^{-1}$ for MWCNTs and 3500 $W \cdot m^{-1} \cdot K^{-1}$ for SWCNTs),[50] h_{IN} is the thickness of the interfacial nanolayer, and r_{CNT} is the radius of a single CNT (Table 1).

After applying the cryogenic protocol, cryo-TEM images revealed a homogeneously distributed, along the nanotube outer walls, interfacial nanolayer of varying thickness. The fragments of the exemplary interfacial nanolayer are marked in red in Figure 4. Note that the nanotube wall cross-sections are straightforwardly visible as highly graphitized straight lines whereas the IL nanolayer forms an isotropic and ubiquitous interface, in terms of the nanotube−interfacial interactions. It must be emphasized that this is the earliest observation of this phenomenon, acquired by means of the unique cryo-TEM imaging procedure, allowing determination of the actual thickness of the interfacial nanolayer.

The analysis of cryo-TEM micrographs confirmed that h_{IN} formed by the adsorption of IL cations and anions around the CNT surface ranged from 1.8 to 10.0 nm with an average value of 4.0 ± 1.7 nm (Figure 4). The average value of h_{IN} was calculated based on more than 150 measurements processed in ImageJ software. Importantly, the h_{IN} values were found as practically independent of the morphological features of the dispersed nanoparticles and were applied to verify the theoretical models.

Hereby, the thermal conductivity k_{IN} of the interfacial nanolayer remained the only unknown parameter of the model developed by Murshed et al.,[26] which cannot be determined by experimental means. According to the literature, its value is several times higher than the thermal conductivity of the base

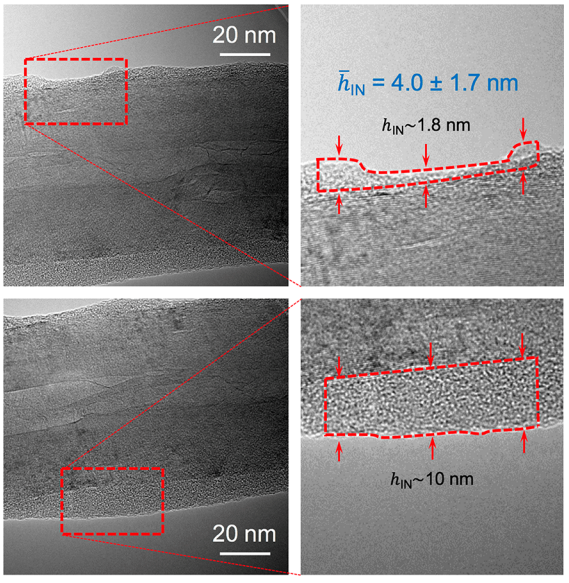

Figure 4. TEM micrographs of in-house 16 h MWCNTs (0.75 wt %) in [EMIM][SCN] recorded after applying the cryogenic protocol, revealing the interfacial nanolayers of the ionic liquid for two different nanotubes. The indicated areas highlight the interfacial nanolayer of varying thickness easily distinguishable from highly graphitized nanotube walls. The straight base of the dashed line figure corresponds to the outermost nanotube walls.

https://dx.doi.org/10.1021/acsami.0c09752
ACS Appl. Mater. Interfaces 2020, 12, 38113−38123

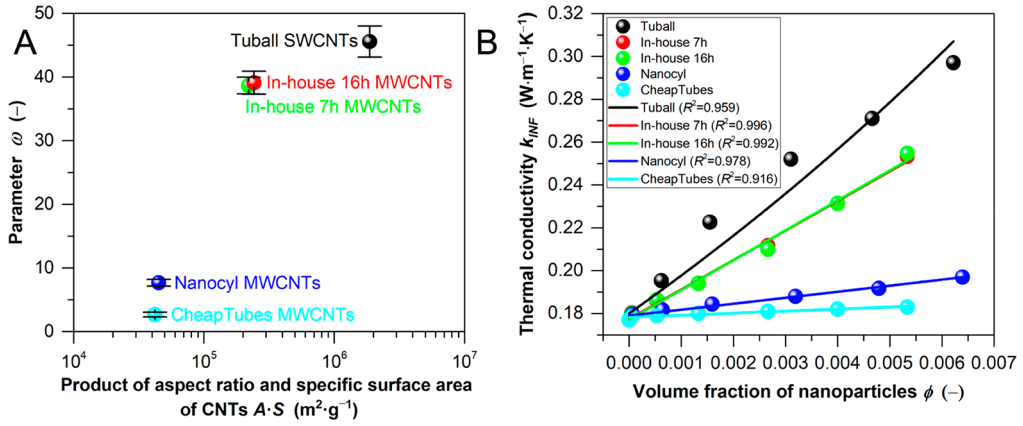

Figure 5. (A) Empirical values of parameter ω representing the ratio of thermal conductivity of the interfacial nanolayer and the ionic liquid (k_{IN}/k_{IL}) for INFs with various CNTs. (B) Comparison of experimental thermal conductivity of INFs at 25 °C (points) with values predicted based on the model developed by Murshed et al.[26] (lines).

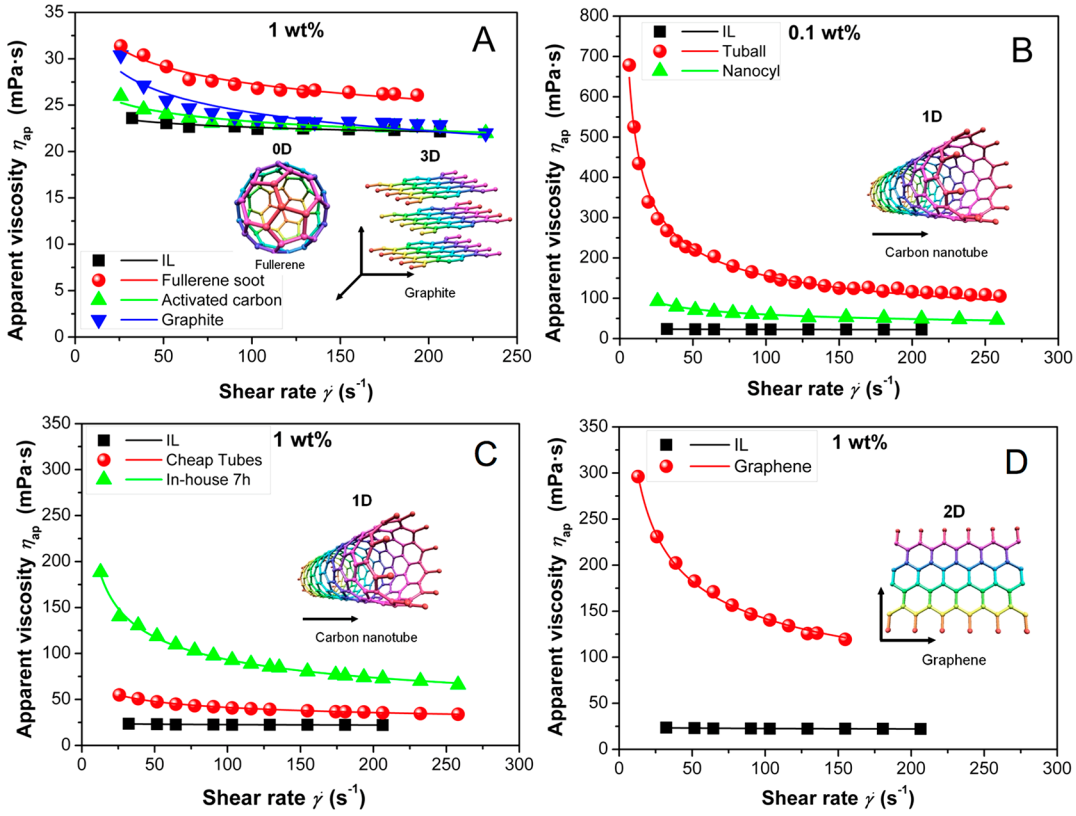

Figure 6. Influence of nanoparticle morphology on the viscosity curves of INFs at 25 °C: (A) 0D fullerene soot, 3D activated carbon, 3D graphite. (B) 1D Tuball SWCNTs, 1D Nanocyl MWCNTs. (C) 1D in-house 7 h MWCNTs, 1D CheapTubes MWCNTs. (D) 2D graphene. Solid lines: Ostwald–de Waele model with parameters given in Table S9 in Supporting Information. Examples of carbon-based nanomaterials reproduced with permission[53] from Elsevier B.V.

liquid.[13,27] However, the orderliness of the ILs absorbed on a CNT surface results in an intermediate thermal conductivity of the interfacial nanolayer: $k_{IL} < k_{IN} < k_{CNT}$.[22] Therefore, the thermal conductivity of the interfacial nanolayer can be expressed as

$$k_{IN} = \omega k_{IL}$$

where $\omega > 1$ is an empirical parameter that depends on the orientation of the IL cations and anions in the solid–liquid interface, as well as the nature and surface chemistry of the CNT. Taking all these factors into account, we have assumed ω as an adjustable parameter. Its value was determined by nonlinear regression analysis of the experimental data using the Nonlinear Curve Fit Tool with the Levenberg–Marquardt algorithm, built in OriginPro software (OriginLab, Northampton, MA). Empirical parameter ω indicated that the thermal conductivity of the interfacial nanolayer was 2.7 to 45.6 times higher than that of the base IL. These values are significantly larger than the results obtained from theoretical formulas or molecular dynamics simulations available in the literature.[30,33,34] Importantly, the values of empirical parameter ω show a logarithmic growth with an increasing product of

https://dx.doi.org/10.1021/acsami.0c09752
ACS Appl. Mater. Interfaces 2020, 12, 38113–38123

aspect ratio and specific surface area ($A \times S$) of the dispersed CNTs (Figure 5A).

It is highly probable that these morphological features of CNTs strongly influenced the orderliness of the IL cations and anions adsorbed on their surface, thereby changing the thermal conductivity of the interface nanolayer. Taking into account all the above characteristics, the model proposed by Murshed et al.[26] accurately predicted the thermal features of INFs with 1D carbon-based nanomaterials (Figure 5B). The calculated coefficient of determination R^2 was close to unity and took values between 0.916 and 0.996.

The enhanced heat transfer capability is, of course, a necessary condition but not sufficient for practical applications of INFs. In industrial practice, optimization is required between heat transfer capabilities and internal resistance arising from the viscosity of transfer fluids.[54] Thus, we have studied the effect of carbon nanomaterial "dimensionality" on the viscosity curves at 25 °C (Figure 6). Note that INFs with 0D and 3D carbon nanomaterials exhibited a more moderate increase in viscosity and rather slight shear thinning properties (Figure 6A) compared to 1D CNTs and 2D graphene sheets (Figure 6B−D). The latter changed the rheological behavior of nanodispersions in a much more significant way (Figures S1 and S2, Supporting Information). Most likely, the 1D and 2D carbon nanoparticles had a stronger affinity to imidazolium cations, providing more ordered structures; hence, the resistance to flow was much higher.[55,56] Furthermore, the relatively high viscosity of the studied INFs was probably related to the well-developed specific surface area and a very large aspect ratio of 1D and 2D carbon-based nanoparticles (Table 1). The significant non-Newtonian, shear thinning behavior of such nanodispersions could have resulted from the reversible disruption of intermolecular interactions, as well as the orientation of nanoparticles in the flow direction, which reduced the flow resistance.[36,55,57] The effect of temperature (25−70 °C) on the viscosity of INFs was tested only for samples containing in-house 7 h MWCNTs. In contrast to pure IL which exhibited Newtonian behavior at each tested temperature (Figure S3A, Supporting Information), the INFs with various loadings of in-house MWCNTs had shear thinning properties in all cases (Figure S3B−E, Supporting Information). Moreover, the viscosity (as well as non-Newtonian behavior) of samples decreased significantly with temperature due to the weakening of intermolecular interactions. For instance, a temperature increase from 25 to 70 °C led to a 65% decrease in the viscosity of pristine [EMIM][SCN] (Table S7 and Figure S3A, Supporting Information). It is consistent with the results reported by Larriba et al.[58] who obtained a 68% increase in viscosity for the same IL, under identical measuring conditions.

The apparent viscosity of INFs with various carbon-based nanomaterials can be successfully described using one of the most popular rheological models, i.e., the Ostwald−de Waele (power-law) formula (solid and dotted lines in Figure 6 and Figures S1−S3). Note that the applied model provided a good description of purely viscous (inelastic), time-independent shear flow of IL and INFs. Calculated parameters of the Ostwald−de Waele model, consistency index K, and flow behavior index n, obtained by the nonlinear regression analysis of experimental data, are summarized in Tables S8 and S9, Supporting Information. Their values confirmed our earlier conclusions that pristine IL and INFs with 0D and 3D carbon nanostructures behaved like Newtonian fluids ($n \approx 1$) with constant (shear-independent) viscosity $\eta_{ap} = K$. Moreover, the INFs with 1D and 2D nanoparticles (≥0.1 wt %) were characterized by relatively high apparent viscosity and strong non-Newtonian, shear thinning (pseudoplastic) properties ($n \ll 1$ and $\eta_{ap} \neq K \neq$ constant). The details of the viscosity results are presented in section S2 in Supporting Information.

CONCLUSIONS

The interfacial nanolayer of IL on the CNT surface, determined experimentally for the first time, had an average thickness of 4.0 nm. Thermal conductivity of the nanolayer was 2.7 to 45.6 times higher than that of the base IL, showing a logarithmic growth with the increasing product of aspect ratio and specific surface area ($A \times S$) of the dispersed CNTs. Predictions by the model of Murshed et al.[26] were in a considerably good agreement with the experimental data of [EMIM][SCN]−CNT nanodispersions.

Our study of carbon nanomaterials of various morphological features on the thermal conductivity of cyano alkylimidazolium-based INFs showed the following: (1) 0D fullerene soot, 3D graphite flakes, and 3D activated carbon practically did not enhance the thermal conductivity of INFs, regardless of their concentration. (2) 2D graphene sheets caused a moderate, linear increase in thermal conductivity of INFs with increasing concentration, up to 7.9% for 1 wt % loading of nanoparticles. (3) 1D CNTs have produced a significant linear increase in the thermal conductivity of INFs with increasing concentration. The maximum enhancement was equal to 67.8% for [EMIM][SCN] + 1 wt % Tuball SWCNTs and 43.9% for [EMIM][SCN] + 1 wt % in-house 16 h MWCNTs. Thermal features of INFs showed a marked enhancement with the increasing product of aspect ratio and specific surface area ($A \times S$) of the dispersed CNTs.

From a rheological point of view, pristine [EMIM][SCN] as well as low-concentration INFs (<0.1 wt %) exhibited Newtonian properties. A higher loading of nanoparticles caused a formation of large carbon agglomerates in the IL, which increased the internal resistance and induced interesting non-Newtonian, pseudoplastic behavior during the steady-shear flow of the samples. 1D CNTs and 2D graphene sheets changed the rheological properties of INFs in a much more significant way compared to 0D and 3D carbon-based nanomaterials, due to their very different morphological features (e.g., extraordinary specific surface area and aspect ratio). Nevertheless, in all cases, the apparent viscosity of INFs increased with nanoparticle concentration, as well as decreased with increasing shear rate and temperature. Equally important, the applied rheological model of Ostwald−de Waele has described the experimental data with satisfying accuracy. Its parameters can be useful in thermal engineering and fluid mechanics, in the description of momentum and heat transfer during laminar/turbulent flow of non-Newtonian INFs. The applied approach constitutes a reliable description for sp^2-C-based in general and, in particular, CNT-based INFs as the most promising systems toward energy management exhibiting the highest thermophysical performance hitherto.

ASSOCIATED CONTENT

Supporting Information

The Supporting Information is available free of charge at https://pubs.acs.org/doi/10.1021/acsami.0c09752.

https://dx.doi.org/10.1021/acsami.0c09752
ACS Appl. Mater. Interfaces 2020, 12, 38113−38123

Tables S1−S9, Figures S1−S3, materials, and experimental results (PDF)

AUTHOR INFORMATION

Corresponding Authors

Marzena Dzida − *University of Silesia in Katowice, Institute of Chemistry, 40-006 Katowice, Poland;* orcid.org/0000-0001-9566-4093; Email: marzena.dzida@us.edu.pl

Sławomir Boncel − *Silesian University of Technology, Department of Organic Chemistry, Bioorganic Chemistry and Biotechnology, 44-100 Gliwice, Poland;* orcid.org/0000-0002-0787-5243; Email: slawomir.boncel@polsl.pl

Authors

Bertrand Jóźwiak − *Silesian University of Technology, Department of Organic Chemistry, Bioorganic Chemistry and Biotechnology, 44-100 Gliwice, Poland*

Grzegorz Dzido − *Silesian University of Technology, Department of Chemical Engineering and Process Design, 44-100 Gliwice, Poland*

Edward Zorębski − *University of Silesia in Katowice, Institute of Chemistry, 40-006 Katowice, Poland;* orcid.org/0000-0001-8152-6693

Anna Kolanowska − *Silesian University of Technology, Department of Organic Chemistry, Bioorganic Chemistry and Biotechnology, 44-100 Gliwice, Poland;* orcid.org/0000-0002-2073-4808

Rafał Jędrysiak − *Silesian University of Technology, Department of Organic Chemistry, Bioorganic Chemistry and Biotechnology, 44-100 Gliwice, Poland*

Justyna Dziadosz − *University of Silesia in Katowice, Institute of Chemistry, 40-006 Katowice, Poland;* orcid.org/0000-0003-4595-6906

Marcin Libera − *University of Silesia in Katowice, Institute of Chemistry, 40-006 Katowice, Poland*

Complete contact information is available at: https://pubs.acs.org/10.1021/acsami.0c09752

Author Contributions

M.D. and S.B. conceived and designed the research; B.J., G.D, E.Z., A.K., R.J., J.D., M.L., S.B., and M.D. conducted the experimental research; B.J. conducted the theoretical research; B.J., S.B. M.D., and E.Z. analyzed the data. The manuscript was written through the contribution of all authors. All authors have given approval to the final version of the manuscript.

Notes

The authors declare no competing financial interest.

ACKNOWLEDGMENTS

This work was financially supported by the National Science Centre (Poland) grant no. 2017/27/B/ST4/02748.

REFERENCES

(1) Bhanushali, S.; Jason, N. N.; Ghosh, P.; Ganesh, A.; Simon, G. P.; Cheng, W. Enhanced Thermal Conductivity of Copper Nanofluids: The Effect of Filler Geometry. *ACS Appl. Mater. Interfaces* **2017**, *9* (22), 18925−18935.

(2) Maxwell, J. C. *A Treatise on Electricity and Magnetism*, 3rd ed.; Clarendon Press: Cambridge, UK, 1891. DOI: 10.1017/CBO9780511709340.

(3) Ribeiro, A. P. C.; Lourenço, M. J. V.; Nieto de Castro, C. A. Thermal Conductivity of Ionanofluids. In *Proceedings of the 17th Symposium on Thermophysical Properties*; June 21−26, 2009, Boulder, CO; Elsevier, 2010.

(4) Nieto de Castro, C. A.; Murshed, S. M. S.; Lourenço, M. J. V.; Santos, F. J. V.; Lopes, M. L. M.; França, J. M. P. Ionanofluids: New Heat Transfer Fluids for Green Processes Development. In *Green Solvents I*; Inamuddin, M. A., Ed.; Springer: Dordrecht, The Netherlands, 2012; pp 233−249. DOI: 10.1007/978-94-007-1712-1_8.

(5) França, J. M. P.; Nieto de Castro, C. A.; Lopes, M. M.; Nunes, V. M. B. Influence of Thermophysical Properties of Ionic Liquids in Chemical Process Design. *J. Chem. Eng. Data* **2009**, *54* (9), 2569−2575.

(6) Tenney, C. M.; Massel, M.; Mayes, J. M.; Sen, M.; Brennecke, J. F.; Maginn, E. J. A Computational and Experimental Study of the Heat Transfer Properties of Nine Different Ionic Liquids. *J. Chem. Eng. Data* **2014**, *59* (2), 391−399.

(7) Chernikova, E. A.; Glukhov, L. M.; Krasovskiy, V. G.; Kustov, L. M.; Vorobyeva, M. G.; Koroteev, A. A. Ionic Liquids as Heat Transfer Fluids: Comparison with Known Systems, Possible Applications, Advantages and Disadvantages. *Russ. Chem. Rev.* **2015**, *84* (8), 875−890.

(8) Musiał, M.; Kuczak, M.; Mrozek-Wilczkiewicz, A.; Musiol, R.; Zorębski, E.; Dzida, M. Trisubstituted Imidazolium-Based Ionic Liquids as Innovative Heat Transfer Media in Sustainable Energy Systems. *ACS Sustainable Chem. Eng.* **2018**, *6* (6), 7960−7968.

(9) Musiał, M.; Malarz, K.; Mrozek-Wilczkiewicz, A.; Musiol, R.; Zorębski, E.; Dzida, M. Pyrrolidinium-Based Ionic Liquids as Sustainable Media in Heat-Transfer Processes. *ACS Sustainable Chem. Eng.* **2017**, *5* (11), 11024−11033.

(10) Holbrey, J. D.; Seddon, K. R. Ionic Liquids. *Clean Technol. Environ. Policy* **1999**, *1* (4), 223−236.

(11) Cherian, T.; Nunes, D. R.; Dane, T. G.; Jacquemin, J.; Vainio, U.; Myllymäki, T. T. T.; Timonen, J. V. I.; Houbenov, N.; Maréchal, M.; Rannou, P.; Ikkala, O. Supramolecular Self-Assembly of Nanoconfined Ionic Liquids for Fast Anisotropic Ion Transport. *Adv. Funct. Mater.* **2019**, *29* (49), 1905054.

(12) Nieto de Castro, C. A.; Ribeiro, A. P. C.; Salome, I. C.; Franca, J. M. P.; Lourenço, M. J. V.; Santos, F. V.; Murshed, S. M. S.; Goodrich, P.; Hardacre, C. Synthesis, Properties and Physical Applications of IoNanofluids. In *Ionic Liquids - New Aspects for the Future*; Kadokawa, J., Ed.; InTech: Rijeka, Croatia, 2013. DOI: 10.5772/52596.

(13) França, J. M. P.; Lourenço, M. J. V.; Murshed, S. M. S.; Pádua, A. A. H.; Nieto de Castro, C. A. Thermal Conductivity of Ionic Liquids and IoNanofluids and Their Feasibility as Heat Transfer Fluids. *Ind. Eng. Chem. Res.* **2018**, *57* (18), 6516−6529.

(14) Pensado, A. S.; Malberg, F.; Gomes, M. F. C.; Pádua, A. A. H.; Fernández, J.; Kirchner, B. Interactions and Structure of Ionic Liquids on Graphene and Carbon Nanotubes Surfaces. *RSC Adv.* **2014**, *4* (35), 18017−18024.

(15) Ettefaghi, E.; Rashidi, A.; Ahmadi, H.; Mohtasebi, S. S.; Pourkhalil, M. Thermal and Rheological Properties of Oil-Based Nanofluids from Different Carbon Nanostructures. *Int. Commun. Heat Mass Transfer* **2013**, *48*, 178−182.

(16) Selvam, C.; Harish, S.; Lal, D. M. Effective Thermal Conductivity and Rheological Characteristics of Ethylene Glycol-Based Nanofluids with Single-Walled Carbon Nanohorn Inclusions. *Fullerenes, Nanotubes, Carbon Nanostruct.* **2017**, *25* (2), 86−93.

(17) Fukushima, T.; Kosaka, A.; Ishimura, Y.; Yamamoto, T.; Takigawa, T.; Ishii, N.; Aida, T. Molecular Ordering of Organic Molten Salts Triggered by Single-Walled Carbon Nanotubes. *Science* **2003**, *300* (5628), 2072−2074.

(18) Fukushima, T.; Aida, T. Ionic Liquids for Soft Functional Materials with Carbon Nanotubes. *Chem. - Eur. J.* **2007**, *13* (18), 5048−5058.

(19) Minea, A. A.; Murshed, S. M. S. A Review on Development of Ionic Liquid Based Nanofluids and Their Heat Transfer Behavior. *Renewable Sustainable Energy Rev.* **2018**, *91*, 584−599.

(20) Murshed, S. M. S.; Nieto de Castro, C. A. Superior Thermal Features of Carbon Nanotubes-Based Nanofluids – A Review. *Renewable Sustainable Energy Rev.* **2014**, *37*, 155–167.
(21) Oster, K.; Hardacre, C.; Jacquemin, J.; Ribeiro, A. P. C.; Elsinawi, A. Thermal Conductivity Enhancement Phenomena in Ionic Liquid-Based Nanofluids (Ionanofluids). *Aust. J. Chem.* **2019**, *72* (2), 21–33.
(22) Nieto de Castro, C. A.; Murshed, S. M. S.; Lourenço, M. J. V.; Santos, F. J. V.; Lopes, M. L. M.; França, J. M. P. Enhanced Thermal Conductivity and Specific Heat Capacity of Carbon Nanotubes Ionanofluids. *Int. J. Therm. Sci.* **2012**, *62*, 34–39.
(23) Zhang, F.-F.; Zheng, F.-F.; Wu, X.-H.; Yin, Y.-L.; Chen, G. Variations of Thermophysical Properties and Heat Transfer Performance of Nanoparticle-Enhanced Ionic Liquids. *R. Soc. Open Sci.* **2019**, *6* (4), 182040.
(24) Ribeiro, A. P. C.; Vieira, S. I. C.; Goodrich, P.; Hardacre, C.; Lourenço, M. J. V.; Nieto de Castro, C. Thermal Conductivity of [Cnmim][(CF3SO2)2N] and [C4mim][BF4] IoNanofluids with Carbon Nanotubes – Measurement, Theory and Structural Characterization. *J. Nanofluids* **2013**, *2* (1), 55–62.
(25) Atashrouz, S.; Mozaffarian, M.; Pazuki, G. Modeling the Thermal Conductivity of Ionic Liquids and Ionanofluids Based on a Group Method of Data Handling and Modified Maxwell Model. *Ind. Eng. Chem. Res.* **2015**, *54* (34), 8600–8610.
(26) Murshed, S. M. S.; Leong, K. C.; Yang, C. Investigations of Thermal Conductivity and Viscosity of Nanofluids. *Int. J. Therm. Sci.* **2008**, *47* (5), 560–568.
(27) Kotia, A.; Borkakoti, S.; Deval, P.; Ghosh, S. K. Review of Interfacial Layer's Effect on Thermal Conductivity in Nanofluid. *Heat Mass Transfer* **2017**, *53* (6), 2199–2209.
(28) Ali, N.; Teixeira, J. A.; Addali, A. A Review on Nanofluids: Fabrication, Stability, and Thermophysical Properties. *J. Nanomater.* **2018**, *2018*, 1–33.
(29) Bastos, A. R. N.; Brites, C. D. S.; Rojas-Gutierrez, P. A.; DeWolf, C.; Ferreira, R. A. S.; Capobianco, J. A.; Carlos, L. D. Thermal Properties of Lipid Bilayers Determined Using Upconversion Nanothermometry. *Adv. Funct. Mater.* **2019**, *29* (48), 1905474.
(30) França, J. M. P.; Nieto de Castro, C. A.; Pádua, A. A. H. Molecular Interactions and Thermal Transport in Ionic Liquids with Carbon Nanomaterials. *Phys. Chem. Chem. Phys.* **2017**, *19* (26), 17075–17087.
(31) Aybar, H. Ş.; Sharifpur, M.; Azizian, M. R.; Mehrabi, M.; Meyer, J. P. A Review of Thermal Conductivity Models for Nanofluids. *Heat Transfer Eng.* **2015**, *36* (13), 1085–1110.
(32) Arthur, O.; Karim, M. A. An Investigation into the Thermophysical and Rheological Properties of Nanofluids for Solar Thermal Applications. *Renewable Sustainable Energy Rev.* **2016**, *55*, 739–755.
(33) Liang, Z.; Tsai, H.-L. Thermal Conductivity of Interfacial Layers in Nanofluids. *Phys. Rev. E* **2011**, *83* (4), No. 041602.
(34) Pal, R. A Novel Method to Determine the Thermal Conductivity of Interfacial Layers Surrounding the Nanoparticles of a Nanofluid. *Nanomaterials* **2014**, *4* (4), 844–855.
(35) Nieto de Castro, C. A.; Lourenço, M. J. V.; Ribeiro, A. P. C.; Langa, E.; Vieira, S. I. C.; Goodrich, P.; Hardacre, C. Thermal Properties of Ionic Liquids and IoNanofluids of Imidazolium and Pyrrolidinium Liquids. *J. Chem. Eng. Data* **2010**, *55* (2), 653–661.
(36) Ferreira, A. G. M.; Simões, P. N.; Ferreira, A. F.; Fonseca, M. A.; Oliveira, M. S. A.; Trino, A. S. M. Transport and Thermal Properties of Quaternary Phosphonium Ionic Liquids and IoNanofluids. *J. Chem. Thermodyn.* **2013**, *64*, 80–92.
(37) Oster, K.; Hardacre, C.; Jacquemin, J.; Ribeiro, A. P. C.; Elsinawi, A. Understanding the Heat Capacity Enhancement in Ionic Liquid-Based Nanofluids (Ionanofluids). *J. Mol. Liq.* **2018**, *253*, 326–339.
(38) Oster, K.; Hardacre, C.; Jacquemin, J.; Ribeiro, A. P. C.; Elsinawi, A. Ionic Liquid-Based Nanofluids (Ionanofluids) for Thermal Applications: An Experimental Thermophysical Characterization. *Pure Appl. Chem.* **2019**, *91* (8), 1309–1340.
(39) Bridges, N. J.; Visser, A. E.; Fox, E. B. Potential of Nanoparticle-Enhanced Ionic Liquids (NEILs) as Advanced Heat-Transfer Fluids. *Energy Fuels* **2011**, *25* (10), 4862–4864.
(40) Liu, J.; Wang, F.; Zhang, L.; Fang, X.; Zhang, Z. Thermodynamic Properties and Thermal Stability of Ionic Liquid-Based Nanofluids Containing Graphene as Advanced Heat Transfer Fluids for Medium-to-High-Temperature Applications. *Renewable Energy* **2014**, *63*, 519–523.
(41) Mahbubul, I. M. *Preparation, Characterization, Properties and Application of Nanofluid*, 1st ed.; Elsevier, Oxford, UK, 2019. DOI: 10.1016/C2016-0-04294-8.
(42) Kolanowska, A.; Kuziel, A.; Li, Y.; Jurczyk, S.; Boncel, S. Rieche Formylation of Carbon Nanotubes – One-Step and Versatile Functionalization Route. *RSC Adv.* **2017**, *7* (81), 51374–51381.
(43) Boncel, S.; Pluta, A.; Skonieczna, M.; Gondela, A.; Maciejewska, B.; Herman, A. P.; Jędrysiak, R. G.; Budniok, S.; Komędera, K.; Błachowski, A.; Walczak, K. Z. Hybrids of Iron-Filled Multiwall Carbon Nanotubes and Anticancer Agents as Potential Magnetic Drug Delivery Systems: In Vitro Studies against Human Melanoma, Colon Carcinoma, and Colon Adenocarcinoma. *J. Nanomater.* **2017**, *2017*, 1262309.
(44) Boncel, S.; Koziol, K. K. K. Enhanced Graphitization of C-CVD Grown Multi-Wall Carbon Nanotube Arrays Assisted by Removal of Encapsulated Iron-Based Phases under Thermal Treatment in Argon. *Appl. Surf. Sci.* **2014**, *301*, 488–491.
(45) Kazakov, A.; Magee, J. W.; Chirico, R. D.; Paulechka, E.; Diky, V.; Muzny, C. D.; Kroenlein, K.; Frenkel, M. *NIST Standard Reference Database 147: Ionic Liquids Database – ILThermo v2.0*; National Institute of Standards and Technology, Gaithersburg, MD, 2017.
(46) Das, S.; Giri, A.; Samanta, S.; Kanagaraj, S. Role of Graphene Nanofluids on Heat Transfer Enhancement in Thermosyphon. *J. Sci. Adv. Mater. Devices* **2019**, *4* (1), 163–169.
(47) Zorębski, E.; Góralski, P. Molar Heat Capacities for (1-Butanol +1,4-Butanediol, 2,3-Butanediol, 1,2-Butanediol, and 2-Methyl-2,4-Pentanediol) as Function of Temperature. *J. Chem. Thermodyn.* **2007**, *39* (12), 1601–1607.
(48) Zorębski, E.; Zorębski, M.; Dzida, M.; Goodrich, P.; Jacquemin, J. Isobaric and Isochoric Heat Capacities of Imidazolium-Based and Pyrrolidinium-Based Ionic Liquids as a Function of Temperature: Modeling of Isobaric Heat Capacity. *Ind. Eng. Chem. Res.* **2017**, *56* (9), 2592–2606.
(49) Zorębski, E.; Musiał, M.; Bałuszyńska, K.; Zorębski, M.; Dzida, M. Isobaric and Isochoric Heat Capacities as Well as Isentropic and Isothermal Compressibilities of Di- and Trisubstituted Imidazolium-Based Ionic Liquids as a Function of Temperature. *Ind. Eng. Chem. Res.* **2018**, *57* (14), 5161–5172.
(50) Balandin, A. A. Thermal Properties of Graphene and Nanostructured Carbon Materials. *Nat. Mater.* **2011**, *10* (8), 569–581.
(51) Holbrey, J. D.; Reichert, W. M.; Reddy, R. G.; Rogers, R. D. Heat Capacities of Ionic Liquids and Their Applications as Thermal Fluids. In *Ionic Liquids as Green Solvents*; ACS Symposium Series; American Chemical Society, 2003; Vol. *856*, pp 121–133. DOI: 10.1021/bk-2003-0856.ch011.
(52) Zaripov, Z. I.; Gumerov, F. M.; Khairutdinov, V. F.; Musiał, M.; Zorębski, E.; Dzida, M.; Abdulagatov, I. M. Thermal Conductivity and Thermal Diffusivity of Pyrrolidinium-BasedIonic Liquids at Atmospheric Pressure. *Fluid Phase Equilib.* **2019**, *485*, 135–145.
(53) Jóźwiak, B.; Boncel, S. Rheology of Ionanofluids – A Review. *J. Mol. Liq.* **2020**, *302*, 112568.
(54) Jamal-Abad, M. T.; Dehghan, M.; Saedodin, S.; Valipour, M. S.; Zamzamian, A. An Experimental Investigation of Rheological Characteristics of Non-Newtonian Nanofluids. *J. Heat Mass Transfer Res.* **2014**, *1* (1), 17–23.
(55) Pamies, R.; Espejo, C.; Carrión, F. J.; Morina, A.; Neville, A.; Bermúdez, M. D. Rheological Behavior of Multiwalled Carbon Nanotube-Imidazolium Tosylate Ionic Liquid Dispersions. *J. Rheol.* **2017**, *61* (2), 279–289.

(56) Pamies, R.; Avilés, M. D.; Arias-Pardilla, J.; Carrión, F. J.; Sanes, J.; Bermúdez, M. D. Rheological Study of New Dispersions of Carbon Nanotubes in the Ionic Liquid 1-Ethyl-3-Methylimidazolium Dicyanamide. *J. Mol. Liq.* **2019**, *278*, 368−375.
(57) Hojjat, M.; Etemad, S. Gh.; Bagheri, R.; Thibault, J. Rheological Characteristics of Non-Newtonian Nanofluids: Experimental Investigation. *Int. Commun. Heat Mass Transfer* **2011**, *38* (2), 144−148.
(58) Larriba, M.; Navarro, P.; García, J.; Rodríguez, F. Selective Extraction of Toluene from N-Heptane Using [Emim][SCN] and [Bmim][SCN] Ionic Liquids as Solvents. *J. Chem. Thermodyn.* **2014**, *79*, 266−271.

https://dx.doi.org/10.1021/acsami.0c09752
ACS Appl. Mater. Interfaces 2020, 12, 38113−38123